SECURITY CLASSIFICATION OF THIS PAGE

REPORT DOCUMENTATION PAGE

AD-A208 902

1a. REPORT SECURITY CLASSIFICATION: UNCLASSIFIED	1b. RESTRICTIVE MARKINGS: NONE
SECURITY CLASSIFICATION AUTHORITY	3. DISTRIBUTION/AVAILABILITY OF REPORT: Approved for public release. Distribution unlimited.
DECLASSIFICATION/DOWNGRADING SCHEDULE	
4. PERFORMING ORGANIZATION REPORT NUMBER(S): Technical Report No. 20	5. MONITORING ORGANIZATION REPORT NUMBER(S)
6a. NAME OF PERFORMING ORGANIZATION: Massachusetts Institute of Technology; 6b. OFFICE SYMBOL (If applicable)	7a. NAME OF MONITORING ORGANIZATION: ONR
6c. ADDRESS (City, State, and ZIP Code): 77 Massachusetts Avenue, Room 1-306, Cambridge, MA 02139	7b. ADDRESS (City, State, and ZIP Code): 800 North Quincy Street, Arlington, VA 22217
8a. NAME OF FUNDING/SPONSORING ORGANIZATION: DARPA; 8b. OFFICE SYMBOL (If applicable)	9. PROCUREMENT INSTRUMENT IDENTIFICATION NUMBER: N00014-86-K-0768
8c. ADDRESS (City, State, and ZIP Code): 1400 Wilson Boulevard, Arlington, VA 22209	10. SOURCE OF FUNDING NUMBERS: PROGRAM ELEMENT NO. R & T Code; PROJECT NO. A 400005; TASK NO.; WORK UNIT ACCESSION NO.

11. TITLE (Include Security Classification)
POLYCRYSTALLINE PLASTIC DEFORMATION AND TEXTURE EVOLUTION FOR CRYSTALS LACKING FIVE INDEPENDENT SLIP SYSTEMS

12. PERSONAL AUTHOR(S)
David M. Parks and Said Ahzi

13a. TYPE OF REPORT	13b. TIME COVERED	14. DATE OF REPORT (Year, Month, Day)	15. PAGE COUNT
Interim Technical	FROM 1988 TO 1989	1989 May 29	44

16. SUPPLEMENTARY NOTATION
Paper submitted for publication to The Journal of the Mechanics and Physics of Solids.

17. COSATI CODES		
FIELD	GROUP	SUB-GROUP

18. SUBJECT TERMS (Continue on reverse if necessary and identify by block number)
Plastic flow in polycrystals, aggregates of insufficient slip systems, simulation of texture evolution. (TTS)

19. ABSTRACT (Continue on reverse if necessary and identify by block number)

We clearly elucidate the kinematic constraints, and the corresponding kinematic indeterminacy of part of the deviatoric stress tensor, in a rigid-viscoplastic single crystal lacking five independent slip systems. The indeterminate stress component is a Lagrange multiplier enforcing the kinematic constraint, and it must be determined from equilibrium considerations. A simple polycrystalline model is constructed which precisely satisfies local kinematic constraints as well as global compatibility. Volume-average global stresses are obtained by approximating the local constraint stress as the corresponding projection of the (to-be-determined) global stress. Applications of the model to hexagonal crystals without pyramidal slip, and to large deformation and texturing of orthorhombic polycrystalline materials (olivine; HDPE) are made.

20. DISTRIBUTION/AVAILABILITY OF ABSTRACT	21. ABSTRACT SECURITY CLASSIFICATION
☒ UNCLASSIFIED/UNLIMITED ☐ SAME AS RPT ☐ DTIC USERS	Unclassified
22a. NAME OF RESPONSIBLE INDIVIDUAL: Dr. Kenneth Wynne	22b. TELEPHONE (Include Area Code): (202) 696-4410; 22c. OFFICE SYMBOL

DD FORM 1473, 84 MAR — 83 APR edition may be used until exhausted. All other editions are obsolete.

SECURITY CLASSIFICATION OF THIS PAGE

POLYCRYSTALLINE PLASTIC DEFORMATION AND TEXTURE EVOLUTION FOR CRYSTALS LACKING FIVE INDEPENDENT SLIP SYSTEMS

D. M. PARKS and S. AHZI
Department of Mechanical Engineering
Massachusetts Institute of Technology
Cambridge, MA 02319

May, 1989

ABSTRACT

We clearly elucidate the kinematic constraints, and the corresponding kinematic indeterminacy of part of the deviatoric stress tensor, in a rigid–viscoplastic single crystal lacking five independent slip systems. The indeterminate stress component is a Lagrange multiplier enforcing the kinematic constraint, and it must be determined from equilibrium considerations. A simple polycrystalline model is constructed which precisely satisfies local kinematic constraints as well as global compatibility. Volume–average global stresses are obtained by approximating the local constraint stress as the corresponding projection of the (to-be-determined) global stress. Applications of the model to hexagonal crystals without pyramidal slip, and to large deformation and texturing of orthrhombic polycrystalline materials (olivine; HDPE) are made.

1. INTRODUCTION

PHYSICALLY–BASED continuum modeling of plastic deformation in polycrystalline aggregates is a broad and active field of research. The simplest effective models of this sort are based on the suggestion of TAYLOR (1938) that local deformation within a heterogeneous polycrystalline aggregate is often approximately homogeneous when a representative material element is subject to loading consistent with macroscopically uniform deformation. This assumption assures both local and global compatibility but in general violates local traction equilibrium across grain boundaries. In many cases, however, major features of both the macroscopic constitutive behavior of the aggregate and the evolution of crystallographic texture with on–going deformation can be accurately simulated by TAYLOR–type models. When applied to crystalline deformation

by slip, various adaptations of the TAYLOR model have provided assessments of effects of differing deformation resistances for different classes of slip systems (HUTCHINSON, 1976; 1977), of self and latent hardening of slip systems (ASARO and NEEDLEMAN, 1985), of strain rate sensitivity of slip (HUTCHINSON, 1976; 1977), and of finite deformation elastic/viscoplastic flow (ASARO and NEEDLEMAN, 1985). Among the effects which cannot be directly addressed by such models are the influences of morphological texture, including grain shape and orientation.

The greatest successes of TAYLOR models have occurred in cubic metal crystals, where the large number of equivalent slip systems which (apart from modest differences due to differential strain hardening) possess equivalent deformation resistances. The flow envelope of a crystal can be defined as the locus of (deviatoric) stress components required to generate resolved shear stresses equal to the deformation resistances on a sufficient set of slip systems so as to accommodate arbitrary deformation rates. For high symmetry cubic metal crystals, the flow envelope is roughly isotropic. In crystals of lower symmetry, where the deformation resistances of different classes of slip systems can vary markedly, the stress required to activate slip systems accommodating an arbitrary deformation rate can become exceedingly high for certain orientations, and the flow envelope can become highly distorted. For this reason, the corresponding polycrystalline aggregate stress levels obtained from TAYLOR type models also become large. In the limiting case of unbounded deformation resistance on all but four or fewer linearly independent slip systems, the TAYLOR estimate of aggregate stress generally becomes unbounded.

HUTCHINSON (1977) noted that the self–consistent method of HILL (1965), as implemented by HUTCHINSON (1970; 1976) could provide reasonable estimates of macro-

scopic flow strength for aggregates of crystals possessing slip systems of widely differing deformation resistance, including the limiting case of less than five linearly independent slip systems. The main reason that the self–consistent model can deal with these cases is that it imposes much less stringent kinematical conditions on the deformation of individual crystals than does the TAYLOR model, with favorably oriented crystals displaying higher deformation than average and unfavorably oriented crystals displaying less deformation than average. HUTCHINSON (1977) applied the self–consistent method to isotropic distributions of hexagonal crystals. Recently TAKESHITA, *et al.*, (1989), using the self–consistent viscoplastic approach of MOLINARI, *et al.*, (1987), modeled the development of crystallographic texture in olivine, an orthorhombic mineral possessing only three independent slip systems.

While many crystalline materials display less than five independent deformation mechanisms (see, for example, GROVES and KELLEY, 1963), our interests in kinematically deficient crystals are motivated by semi–crystalline polymers such as high density polyethylene (HDPE), Nylon–6, and polyethylene teraphthalate (PET). The crystalline domains of these materials, while belonging to different crystal classes (orthorhombic, monoclinic, and triclinic, respectively), nonetheless share the feature that material elements aligned with the lattice directions corresponding to the stiff covalent bonding of the backbone polymer chain are plastically *inextensible*. That is, all known mechanisms of plastic deformation in these materials, including slip (and, where applicable, twinning and martensitic transformation), leave material distances along the chain axis invariant. Large plastic deformation of semi–crystalline polymers can impart significant crystallographic texture to these materials. A common textural feature is that the crystallographic chain axes preferentially align with the material axes of maximum stretch

(BOWDEN and YOUNG, 1974; HAUDIN, 1982). As this process occurs, the macroscopic stress required to sustain plastic flow can ultimately rise sharply as the locally available sites for continued macroscopic extension are geometrically deactivated.

Our attempts to model large deformation in HDPE using the self–consistent formulation of MOLINARI, *et al.*, (1987) provided qualitatively correct deformation textures, but unsatisfactory macroscopic stress–strain behavior; macroscopic average deviatoric stress components showed extreme fluctuations, especially at sharper textures. Because of the local inextensibility constraint, the incompressible viscoplastic formulation of MOLINARI, *et al.*, (1987) cannot fully resolve the local deviatoric stress within a crystallographic inclusion, and the erratic macroscopic stresses reflect this local indeterminacy. It seems that HUTCHINSON (1977) avoided this difficulty by using a slightly different numerical formulation of the self–consistent model, including a slight elastic compressibility.

Here we clearly identify the kinematically indeterminate component of stress deviator in a rigid–viscoplastic crystal possessing a kinematic rank deficiency (*e.g.*, a locally inextensible direction). This portion of local stress state must be determined from equilibrium considerations, and procedures for so doing are similar to (but not identical with) those for obtaining hydrostatic pressure in incompressible materials.The focus of the paper is the development of a new hybrid formulation to estimate the local deviatoric constraint stresses in terms of the (to–be–determined) macroscopic stress. The complete system of equations, which we term the constrained hybrid (CH) model, possesses a simple mathematical structure. The model is closely akin to the simple TAYLOR model for crystals of full kinematic rank so that, for example, rate problems of imposed macroscopic deformation can be solved without global iterations, in con-

trast to more elaborate self–consistent models. Large deformation texture predictions and macroscopic stress–strain behavior are readily obtained.

We compare the model with calculations of HUTCHINSON (1977) for isotropic textures of hexagonal crystals possessing only four independent systems. We generalize the CH model to cases of three or fewer slip systems (two or more deviatoric constraints) and compare results of the model with the texture predictions of TAKESHITA, *et al.*, (1989) in olivine. Finally, we apply the CH model in a highly idealized way to the deformation of initially isotropic HDPE.

Notation is based on the following conventions. Scalars are in mathematical italics (A, a, α), vectors are lower case bold-face ($\mathbf{a}$), second order tensors are upper case bold–face ($\mathbf{A}$), and fourth order tensors are in upper case caligraphic type ($\mathcal{A}$). Tensor (dyadic) products are indicated by '$\otimes$' and tensor scalar products of appropriate order are denoted by a raised dot. The superscripts "$\prime$","T", and "-1" denote "deviatoric part of", "transpose", and "inverse", respectively. When required, repeated cartesian subscripts are summed from 1 to 3. For example, on orthonormal basis vectors $\mathbf{e}_i$:

$$\left.\begin{array}{l}\mathbf{c} = c_i\mathbf{e}_i \\ \mathbf{a} = a_i\mathbf{e}_i\end{array}\right. \quad \Rightarrow \quad \mathbf{a}\cdot\mathbf{c} = a_i c_i$$

$$\left.\begin{array}{l}\mathbf{A} = A_{ij}\mathbf{e}_i\otimes\mathbf{e}_j \\ \mathbf{B} = B_{ij}\mathbf{e}_i\otimes\mathbf{e}_j\end{array}\right. \quad \Rightarrow \quad \left\{\begin{array}{l}\mathbf{Ac} = A_{ij}c_j\,\mathbf{e}_i \\ \mathbf{AB} = A_{ik}B_{kj}\,\mathbf{e}_i\otimes\mathbf{e}_j \\ \mathbf{A}\cdot\mathbf{B} = tr\mathbf{A}\mathbf{B}^T = A_{ij}B_{ij}\end{array}\right.$$

$$\left.\begin{array}{l}\mathcal{A} = \mathbf{B}\otimes\mathbf{C} \\ \mathcal{B} = \mathbf{D}\otimes\mathbf{E}\end{array}\right. \quad \Rightarrow \quad \left\{\begin{array}{l}\mathcal{A}\,[\mathbf{G}] = \mathbf{B}\,(\mathbf{C}\cdot\mathbf{G}) \\ \mathcal{A}\mathcal{B} = (\mathbf{C}\cdot\mathbf{D})\,\mathbf{B}\otimes\mathbf{E}.\end{array}\right.$$

2. CONSTRAINED SINGLE CRYSTAL

Consider a crystal possessing N slip systems, of which the αth possesses slip plane normal $\mathbf{n}^\alpha$ and slip direction $\mathbf{s}^\alpha$, with $\mathbf{n}^\alpha \cdot \mathbf{s}^\alpha = 0$. Let the shear strain rate on system α be $\dot{\gamma}^\alpha$. In anticipation of large deformation we neglect elasticity and take $\mathbf{D}$, the traceless rate of deformation generated by these slips, to be given by

$$\begin{aligned} \mathbf{D} &= \sum_{\alpha=1}^{N} \dot{\gamma}^\alpha \, \frac{1}{2} \{ \mathbf{n}^\alpha \otimes \mathbf{s}^\alpha + \mathbf{s}^\alpha \otimes \mathbf{n}^\alpha \} \\ &\equiv \sum_{\alpha=1}^{N} \dot{\gamma}^\alpha \, \mathbf{R}^\alpha, \end{aligned} \tag{1}$$

where $\mathbf{R}^\alpha$ is the symmetric, traceless Schmid tensor associated with slip system α.

We further assume that the span of the N tensors $\mathbf{R}^\alpha$ has, in symmetric deviatoric second order tensor space, T_2', a kinematic deficiency of rank one; that is, a single constraint (in addition to incompressibility) exists on $\mathbf{D}$. As a physical example of such a constraint, suppose that material fibers parallel to unit vector $\mathbf{c}$ are inextensible. Such a constraint can arise in hexagonal crystals when pyramidal slip is absent and only basal and prismatic slip are available; in this case the inextensible fiber coincides with [0001] directions, HUTCHINSON (1977). The inextensibility constraint can be written as

$$\mathbf{c} \cdot \mathbf{D}\mathbf{c} = 0. \tag{2}$$

In order for this to be so for arbitrary shears $\dot{\gamma}^\alpha$, it is necessary that $\mathbf{c} \cdot \mathbf{R}^\alpha \mathbf{c} = 0$ for each system. These constraints can also be phrased in terms of the tensor scalar product of $\mathbf{D}$ (or $\mathbf{R}^\alpha$) with the tensorial internal variable $\mathbf{C} = \mathbf{c} \otimes \mathbf{c}$. The tensor $\mathbf{C}$ is not irreducible, and we find it more convenient to retain the traceless symmetric second order tensor $\mathbf{C}' \equiv \mathbf{C} - \frac{1}{3}\mathbf{I}$, where $\mathbf{I}$ is the second order identity tensor, as local internal

variable. Because $\mathbf{D}$ and $\mathbf{R}^\alpha$ are traceless, the inextensibility constraint (2) can also be expressed as

$$\mathbf{D} \cdot \mathbf{C}' = 0, \tag{3}$$

implying

$$\mathbf{R}^\alpha \cdot \mathbf{C}' = 0. \tag{4}$$

In view of the constraints (4), we will denote the span of $\mathbf{R}^\alpha$ by $T'_{2\perp C}$, a four dimensional subspace of T'_2 which is orthogonal to the one dimensional subspace spanned by $\mathbf{C}'$.

We now specify viscoplastic constitutive equations for the shears, $\dot{\gamma}^\alpha$. Following many others (*e.g.*, HUTCHINSON, 1976; PAN and RICE, 1983; ASARO and NEEDLEMAN, 1985), we assume that $\dot{\gamma}^\alpha$ depends on the resolved shear stress through a power law relation of the form

$$\dot{\gamma}^\alpha = \dot{\gamma}_0 \, \frac{\tau^\alpha}{g^\alpha} \, \left|\frac{\tau^\alpha}{g^\alpha}\right|^{n-1}, \tag{5}$$

where n is the rate exponent, g^α is the slip system hardness (or shear strength), $\dot{\gamma}_0$ is a pre-multiplying strain rate, and τ^α ($\leq g^\alpha$), the resolved shear stress on system α, is given by

$$\tau^\alpha = \mathbf{T} \cdot \mathbf{R}^\alpha, \tag{6}$$

where $\mathbf{T}$ is the Cauchy stress. Since $\mathbf{R}^\alpha$ is deviatoric, we can also express the resolved shear stress as $\tau^\alpha = \mathbf{S} \cdot \mathbf{R}^\alpha$, where the stress deviator is $\mathbf{S} = \mathbf{T} - \frac{1}{3} tr(\mathbf{T})\, \mathbf{I}$. Slip system strength may evolve with deformation according to

$$\dot{g}^\alpha = \sum_{\beta=1}^{N} h^{\alpha\beta} \, |\dot{\gamma}^\beta|, \tag{7}$$

where $h^{\alpha\beta}$ is a matrix of hardening moduli.

The stress deviator $\mathbf{S}$ can be uniquely decomposed as

$$\begin{aligned} \mathbf{S} &= \mathbf{S}^* + S_C \mathbf{C}' \\ &= \mathbf{S}^* + \frac{3}{2} (\mathbf{S} \cdot \mathbf{C}') \, \mathbf{C}', \end{aligned} \tag{8}$$

where $\mathbf{S}^* \in T'_{2 \perp C}$; that is, $\mathbf{S}^* \cdot \mathbf{C}' = 0$. Using (6) and (8), the resolved shear stress can also be expressed as

$$\begin{aligned} \tau^\alpha &= \mathbf{S}^* \cdot \mathbf{R}^\alpha + \frac{3}{2} (\mathbf{S} \cdot \mathbf{C}') \, \mathbf{C}' \cdot \mathbf{R}^\alpha \\ &= \mathbf{S}^* \cdot \mathbf{R}^\alpha, \end{aligned} \tag{10}$$

because of (4). When (10) is inserted into (5), and the expression for $\dot{\gamma}^\alpha$ inserted into (1), the deformation rate can be written as

$$\begin{aligned} \mathbf{D} &= \left\{ \dot{\gamma}_0 \sum_{\alpha=1}^{N} \frac{1}{g^\alpha} \left(\left| \frac{\mathbf{S}^* \cdot \mathbf{R}^\alpha}{g^\alpha} \right| \right)^{n-1} \mathbf{R}^\alpha \otimes \mathbf{R}^\alpha \right\} [\mathbf{S}^*] \\ &\equiv \mathcal{M}(\mathbf{S}^*) \, [\mathbf{S}^*]. \end{aligned} \tag{11}$$

The deformation rate is *independent of the part of the stress deviator lying outside* $T'_{2 \perp C}$. Many models of crystallographic slip neglect effects of hydrostatic stress on slip rates. Thus the independence of the deformation rate from a part of the stress tensor is not entirely without precedent. In the formulation of boundary value problems of incompressible crystalline slip, the incompressibility condition $\mathbf{I} \cdot \mathbf{D} = 0$ is viewed as a constraint and the hydrostatic stress $\sigma \equiv \mathbf{I} \cdot \mathbf{T} / (\mathbf{I} \cdot \mathbf{I}) = \frac{1}{3} \mathbf{I} \cdot \mathbf{T}$ is a Lagrange multiplier enforcing the constraint, the latter being determined from equilibrium considerations. Analogously, in kinematically deficient crystals, $\mathbf{D} \cdot \mathbf{C}' = 0$ is a constraint, and the enforcing Lagrange multplier $S_C = \mathbf{C}' \cdot \mathbf{T} / (\mathbf{C}' \cdot \mathbf{C}') = \frac{3}{2} \mathbf{C}' \cdot \mathbf{S}$ must be determined from equilibrium.

Thus, there are two main features which distinguish the viscoplastic response of the constrained crystal from that of "traditional" crystals. First, the deformation rate lies in a four-dimensional subspace, $T'_{2\perp C}$, of deviatoric space, T'_2, rather than, in general, spanning the latter. Secondly, the deformation does not depend on the entire deviatoric stress, but rather on only the part $\mathbf{S}^*$ lying in a four-dimensional deviatoric subspace. Given these facts, it is clear that the convexity (implying $\mathbf{D}/\mathbf{S}$ invertibility) and shear rate uniqueness properties (HILL, 1956) usually associated with power law viscoplastic single crystal slip models (*e.g.*, HUTCHINSON, 1976) fail to hold. However, *local* convexity connecting the respective four-dimensional subspaces, implying $\mathbf{D}/\mathbf{S}^*$ invertibility, does obtain. We will now use these properties and observations regarding the constrained single crystal model in formulating a polycrystalline model of deformation.

3. POLYCRYSTALLINE AGGREGATE

3.1 Kinematics

Consider an aggregate of crystals of the type described in the previous section which occupy the domain Ω of volume V_Ω. We imagine that for points $\mathbf{x}$ on the boundary $\partial\Omega$, the velocity $\mathbf{v}$ is prescribed according to

$$\mathbf{v} = \bar{\mathbf{L}}\mathbf{x} = \left(\bar{\mathbf{D}} + \bar{\mathbf{W}}\right)\mathbf{x}. \tag{12}$$

Here $\bar{\mathbf{L}}$ is a constant macroscopic "velocity gradient" tensor with symmetric part $\bar{\mathbf{D}} = \frac{1}{2}\left(\bar{\mathbf{L}} + \bar{\mathbf{L}}^T\right)$ and skew part $\bar{\mathbf{W}} = \frac{1}{2}\left(\bar{\mathbf{L}} + \bar{\mathbf{L}}^T\right)$. Incompressibility dictates that $tr\bar{\mathbf{L}} = tr\bar{\mathbf{D}} = 0$.

Within an individual crystal, let the axis of inextensibility be parallel to the unit vector $\mathbf{c}$. The local deformation rate $\mathbf{D}$ within such a crystal must satisfy the constraints (3,4).

Following the insight of TAYLOR, we would like to choose a local $\mathbf{D}$ which, while satisfying (3,4), is nonetheless "close" to the macroscopically imposed $\bar{\mathbf{D}}$. A minimal requirement of global compatibility within the aggregate (*e.g.*, HILL, 1972) is that the volume average deformation rate, given by

$$< \mathbf{D} > \equiv \frac{1}{V_\Omega} \int_{V_\Omega} \mathbf{D}\, dV, \tag{13}$$

equals $\bar{\mathbf{D}}$:

$$< \mathbf{D} > \;=\; \bar{\mathbf{D}}. \tag{14}$$

In order to choose local values of $\mathbf{D}$ which satisfy (3,14), let us first introduce the "intermediate" traceless deformation rate $\tilde{\mathbf{D}}$, given by

$$\tilde{\mathbf{D}} \equiv \mathcal{K}\left[\bar{\mathbf{D}}\right], \tag{15}$$

where $\mathcal{K}$ is a constant fourth order tensor (to be specified below) mapping T_2' into itself.

We propose to express $\mathbf{D}$ as

$$\mathbf{D} = \tilde{\mathbf{D}} - d\,\mathbf{C}', \tag{16}$$

where d is a constant which can be evaluated by enforcing (3):

$$0 = \mathbf{D}\cdot\mathbf{C}' = \tilde{\mathbf{D}}\cdot\mathbf{C}' - d\,\mathbf{C}'\cdot\mathbf{C}', \tag{17}$$

so that

$$d = \frac{\tilde{\mathbf{D}}\cdot\mathbf{C}'}{\mathbf{C}'\cdot\mathbf{C}'} = \frac{3}{2}\tilde{\mathbf{D}}\cdot\mathbf{C}'. \tag{18}$$

On combining (16) with (18), we obtain

$$\begin{aligned}\mathbf{D} &= \tilde{\mathbf{D}} - \frac{3}{2}\mathbf{C}'\left(\tilde{\mathbf{D}}\cdot\mathbf{C}'\right)\\ &= \left\{\mathcal{I} - \frac{3}{2}\mathbf{C}'\otimes\mathbf{C}'\right\}\left[\tilde{\mathbf{D}}\right]\\ &\equiv \mathcal{P}\left[\tilde{\mathbf{D}}\right].\end{aligned} \tag{19}$$

Here $\mathcal{I}$ is the fourth order identity tensor and $\mathcal{P}$ is the local fourth order "projection" tensor mapping T_2' into $T_{2\perp C}'$. The geometric interpretation of (16–19) is shown schematically in Fig. 1.

We note in passing that $\mathbf{D}$, as defined by (19), is the unique element of $T_{2\perp C}'$ closest to $\tilde{\mathbf{D}}$ (min $|\tilde{\mathbf{D}} - \mathbf{D}|$). For those crystals having $\tilde{\mathbf{D}}\cdot\mathbf{C}' = 0$, $\mathbf{D} = \tilde{\mathbf{D}}$, analogous to the TAYLOR assumption in unconstrained crystals.

Now, by inserting (19) into the global average compatibility condition (14), and recalling that $\tilde{\mathbf{D}}$ is constant, we obtain

$$< P \left[\tilde{\mathbf{D}}\right] > = < P > \left[\tilde{\mathbf{D}}\right] = \bar{\mathbf{D}}. \tag{20}$$

A comparison of (20) with (15) indicates that

$$K = < P >^{-1}, \tag{21}$$

so that local deformation is

$$\mathbf{D} = \left\{P < P >^{-1}\right\} \left[\tilde{\mathbf{D}}\right]. \tag{22}$$

We complete the description of local kinematics by choosing the local spin $\mathbf{W}$. As in TAYLOR models which take no account of morphological grain texture, we simply equate local spin with the global average spin:

$$\mathbf{W} = \bar{\mathbf{W}}, \tag{23}$$

trivially satisfying $< \mathbf{W} > = \bar{\mathbf{W}}$. The rate of change of lattice orientation is given by a spin tensor $\mathbf{W} - \mathbf{W}^p$ which provides the following evolution equations (ASARO and RICE, 1977) for $\mathbf{R}^\alpha$ and for $\mathbf{A}^\alpha$, the latter of which is the skew part of the slip system dyadic:

$$\dot{\mathbf{R}}^\alpha = (\mathbf{W} - \mathbf{W}^p)\mathbf{R}^\alpha - \mathbf{R}^\alpha(\mathbf{W} - \mathbf{W}^p), \tag{24}$$

$$\dot{\mathbf{A}}^\alpha = (\mathbf{W} - \mathbf{W}^p)\mathbf{A}^\alpha - \mathbf{A}^\alpha(\mathbf{W} - \mathbf{W}^p), \tag{25}$$

where the plastic spin, $\mathbf{W}^p$, within a crystal is given by

$$\begin{aligned} \mathbf{W}^p &= \sum_{\alpha=1}^{N} \dot{\gamma}^\alpha \frac{1}{2} \{\mathbf{n}^\alpha \otimes \mathbf{s}^\alpha - \mathbf{s}^\alpha \otimes \mathbf{n}^\alpha\} \\ &\equiv \sum_{\alpha=1}^{N} \dot{\gamma}^\alpha \mathbf{A}^\alpha. \end{aligned} \tag{26}$$

We note in passing that the tensor $\mathbf{C}'$, being connected to the crystal lattice, also evolves with this spin:

$$\dot{\mathbf{C}}' = (\mathbf{W} - \mathbf{W}^p)\mathbf{C}' - \mathbf{C}'(\mathbf{W} - \mathbf{W}^p). \tag{27}$$

3.2 Stress and Equilibrium

The macroscopic stress deviator $\bar{\mathbf{S}}$ must also be the volume average of the local stress deviators:

$$< \mathbf{S} > \quad = \quad \bar{\mathbf{S}}. \tag{28}$$

On inserting the decomposition for $\mathbf{S}$ given by (8) into (28), we obtain

$$< \mathbf{S}^* > + \frac{3}{2} < (\mathbf{S} \cdot \mathbf{C}')\mathbf{C}' > \quad = \quad \bar{\mathbf{S}}. \tag{29}$$

The local stresses $\mathbf{S}^*$ are determined in terms of $\bar{\mathbf{D}}$ by inserting (22) into (11) and then inverting the latter equation. However, the local deviatoric stress component $S_C = \frac{3}{2}\mathbf{S}\cdot\mathbf{C}'$ is a reaction enforcing the inextensibility constraint and can be determined only from *equilibrium* considerations. We approximate this local stress component as the corresponding projection (component) of the macroscopic stress, $\bar{\mathbf{S}}$:

$$S_C = \frac{3}{2}\mathbf{S} \cdot \mathbf{C}' \doteq \frac{3}{2}\bar{\mathbf{S}} \cdot \mathbf{C}'. \tag{30}$$

When (30) is inserted into (29), and the equation is rearranged (bearing in mind that $\bar{\mathbf{S}}$ is constant), there obtains

$$\begin{aligned} < \dot{\mathbf{S}}^* > \quad &= \quad \left\{ I - \frac{3}{2} < \mathbf{C}' \otimes \mathbf{C}' > \right\} [\bar{\mathbf{S}}] \\ &= \quad < \mathcal{P} > [\bar{\mathbf{S}}]. \end{aligned} \tag{31}$$

Equation (31) provides the connection between global deformation rate and stress deviator. As has been emphasized by others (*e.g.*, ASARO, 1983a,b), the simulation of

deformation and texture evolution in general should not proceed by prescribing *a priori* all components of $\bar{\mathbf{D}}$. Rather, specific components of $\bar{\mathbf{D}}$ and of $\bar{\mathbf{S}}$ must be given in a manner consistent with a well posed boundary value problem. For example, in simple compression, one might prescribe $\bar{D}_{33} = \dot{E} \neq 0$ and require $\bar{S}_{31} = \bar{S}_{32} = \bar{S}_{11} - \bar{S}_{22} = \bar{S}_{12} = 0$. In any event, the five prescribed macroscopic components, in conjunction with the five relations (31), provide the means for determining all stress deviators and deformation rates, both locally and in global average.

8.8 Tensorial Representation of Texture

In our constrained hybrid model, the macroscopic texture tensor $< P >$ plays a prominent role in defining both the local kinematics and global equilibrium. This tensor can be explicitly evaluated by replacing the volume integral in its definition by a weighted integration over orientations defined on the unit sphere, S. ONAT and LECKIE (1988) have recently given a convenient tensorial representation for a scalar field on S. Here we adapt those results for the polycrystalline aggregate.

Let an ensemble of N_g grains of equal volume constituting a material point have c–axis unit vectors $(\pm\mathbf{c}_1, \pm\mathbf{c}_2, \ldots, \pm\mathbf{c}_{N_g})$, where we note that the $\pm$ sign is necessary since the symmetry of an axis emphasizes that no unique sign can be assigned to $\mathbf{c}_i$. The endpoints of this set of unit vectors pierce S at $2N_g$ locations. We describe the cloud of points on S by an axis orientation density function, $\nu_{\mathbf{C}}(\mathbf{n})$. Consider a given point, $\mathbf{n}$, on S and surround it with an infinitesimal area $\mathrm{d}A$. Let $\mathrm{d}N_g$ be the number of grains with c–axis projecting into $\mathrm{d}A$; the point density $\mathrm{d}N_g/\mathrm{d}A$ is normalized to obtain $\nu_{\mathbf{C}}(\mathbf{n})$:

$$\nu_{\mathbf{C}}(\mathbf{n}) \equiv \frac{2\pi}{N_g} \frac{\mathrm{d}N_g}{\mathrm{d}A}. \tag{32}$$

ONAT and LECKIE (1988) have shown that functions $\nu_{\mathbf{C}}$ of this sort can be represented in the form

$$\nu_{\mathbf{C}}(\mathbf{n}) = 1 + \bar{C}'_{ij} F_{ij}(\mathbf{n}) + \bar{C}_{ijkl} \mathcal{F}_{ijkl}(\mathbf{n}) + \dots \tag{33}$$

where

$\bar{C}'_{ij}$: cartesian components of a traceless, symmetric second order tensor ($\bar{C}'_{ij} = \mathbf{e}_i \cdot \bar{C}' \mathbf{e}_j$)

$\bar{C}_{ijkl}$: cartesian components of a fourth order completely symmetric, completely traceless tensor, *etc.*,

and the even Fourier "basis" terms are modified spherical functions having cartesian components

$$F_{ij}(\mathbf{n}) \equiv n_i n_j - \frac{1}{3}\delta_{ij}, \tag{34}$$

$$\mathcal{F}_{ijkl}(\mathbf{n}) \equiv \left\{ \begin{array}{c} n_i n_j n_k n_l \\ -\frac{1}{7}\left(\delta_{ij} n_k n_l + \delta_{kl} n_i n_j + \delta_{ik} n_j n_l + \delta_{il} n_j n_k + \delta_{jk} n_i n_l + \delta_{jl} n_i n_k\right) \\ +\frac{1}{5\times 7}\left(\delta_{ij}\delta_{kl} + \delta_{ik}\delta_{jl} + \delta_{il}\delta_{jk}\right) \end{array} \right\}, \tag{35}$$

etc.

Here δ_{ij} is the Kronecker delta, and n_i are cartesian components of the unit vector $\mathbf{n}$ relative to the orthonormal basis $\mathbf{e}_i$. In direct tensor notation, for example, $\mathbf{F}(\mathbf{n}) = \mathbf{n} \otimes \mathbf{n} - \frac{1}{3}\mathbf{I}$.

The basis tensors $\mathbf{F}$, $\mathcal{F}$, ... generate their corresponding Fourier coefficients through

$\nu_{\mathbf{c}}(\mathbf{n})$:

$$1 = \frac{1}{4\pi}\int_S \nu_{\mathbf{c}}(\mathbf{n}) \times 1 \, \mathrm{d}A, \tag{36}$$

$$\bar{C}'_{ij} = \frac{1}{4\pi} \times \frac{3 \times 5}{2} \int_S \nu_{\mathbf{c}}(\mathbf{n}) \times F_{ij}(\mathbf{n}) \, \mathrm{d}A, \tag{37}$$

$$\bar{C}_{ijkl} = \frac{1}{4\pi} \times \frac{3 \times 5 \times 7 \times 9}{2 \times 3 \times 4} \int_S \nu_{\mathbf{c}}(\mathbf{n}) \times \mathcal{F}_{ijkl}(\mathbf{n}) \, \mathrm{d}A, \tag{38}$$

etc.

The Fourier coefficients $\bar{C}'_{ij}$, $\bar{C}_{ijkl}$, ... can be thought of as "moments" of the axis orientation distribution function, $\nu_{\mathbf{c}}(\mathbf{n})$. ONAT and LECKIE emphasize that the tensor character of the Fourier coefficients is such that, under orthogonal transformations $\mathbf{Q}$, they transform via standard tensor transformations of appropriate order, *e.g.*, $\bar{\mathbf{C}}' \rightarrow \mathbf{Q}\bar{\mathbf{C}}'\mathbf{Q}^T$, *etc.* For isotropic distributions of the c–axis, $\nu_{\mathbf{c}}(\mathbf{n}) = 1$, and all other texture tensors ($\bar{\mathbf{C}}'$, $\bar{\mathcal{C}}$, *etc.*) vanish.

We can use the Fourier tensors to calculate those ensemble–average tensor functions of the texture which depend only on the local c–axis orientation by evaluating the integral over S of the function, weighted by $\nu_{\mathbf{c}}(\mathbf{n})$; *i.e.*,

$$< \hat{T}(\mathbf{c}) > \equiv \frac{1}{4\pi}\int_S \nu_{\mathbf{c}}(\mathbf{n}) \; \hat{T}(\mathbf{n}) \, \mathrm{d}A \tag{39}$$

for any tensor–valued function $\hat{T}(\mathbf{c})$. In the particular case of the projection tensor P,

$$\begin{aligned} P(\mathbf{c}) &= I - \frac{3}{2}\left(\mathbf{c}\otimes\mathbf{c} - \frac{1}{3}\mathbf{I}\right) \otimes \left(\mathbf{c}\otimes\mathbf{c} - \frac{1}{3}\mathbf{I}\right) \\ &= I - \frac{3}{2}\mathbf{F}(\mathbf{c}) \otimes \mathbf{F}(\mathbf{c}). \end{aligned} \tag{40}$$

We can define the average value, $< P >$, by its action on an arbitrary $\mathbf{G} \in T_2'$. On

using (33–40), the result can be expressed as

$$< P > [\mathbf{G}] = \left\{ \begin{array}{c} \frac{4}{5}\mathbf{G} \\ +\frac{3\times4}{5\times7\times9}\left(\bar{\mathbf{C}}'\cdot\mathbf{G}\right)\mathbf{I} - \frac{2}{5\times7}\left\{\bar{\mathbf{C}}'\mathbf{G} + \mathbf{G}\bar{\mathbf{C}}'\right\} \\ -\frac{3\times4}{5\times7\times9}\,\bar{C}\,[\mathbf{G}] \end{array} \right\} \tag{41}$$

precisely, independent of any higher Fourier moment of texture. For isotropic distribution of the c–axis, $\bar{\mathbf{C}}' = \bar{C} = 0$. In such cases, for example, from (15), (21), and (41), $< P > [\tilde{\mathbf{D}}] = \frac{4}{5}\tilde{\mathbf{D}}$ so that $\tilde{\mathbf{D}} = \frac{5}{4}\bar{\mathbf{D}}$.

The tensor mapping on the unit sphere presumes a smoothed, infinite dimensional basis for the axis orientation distribution, whereas the motivation (and, indeed, numerical simulations of polycrystals) are based on a finite number of grains. Rational, effective means for obtaining the smoothed texture tensors $\bar{\mathbf{C}}'$, $\bar{C}$, *etc.*, from finite populations have been developed based on invariant tesselation and quadrature on the manifold S, PARKS (1989).

3.4 Generalization to Two or More Constraints

The method outlined in sections 3.1 and 3.2 is applicable to polycrystalline models of crystals having a single kinematic deficiency in deviatoric response. We briefly generalize the formulation to accommodate crystals having two linearly independent constraints on deviatoric deformation; further generalization to three or more constraints is transparent. The extended model forms the basis for simulations of deformation and texture evolution in polycrystalline olivine reported in section 4.3, below.

Suppose that deformation in a crystal satisfies the condition $\mathbf{D}\cdot\mathbf{B}' = 0$ in addition

to (3), where the deviatoric tensor $\mathbf{B}'$ is orthogonal to $\mathbf{C}'$: $\mathbf{B}' \cdot \mathbf{C}' = 0$. We again introduce the intermediate tensor $\tilde{\mathbf{D}}$ using (15), but generalize (16) to

$$\mathbf{D} = \tilde{\mathbf{D}} - d\,\mathbf{C}' - b\,\mathbf{B}'. \tag{42}$$

Enforcement of the two constraints provides $b = (\tilde{\mathbf{D}} \cdot \mathbf{B}')/(\mathbf{B}' \cdot \mathbf{B}')$ as well as the result (18) for d. The generalization of (19) is

$$\mathbf{D} = \mathcal{R}\,[\tilde{\mathbf{D}}], \tag{43}$$

where

$$\mathcal{R} = \mathcal{P} - \frac{1}{(\mathbf{B}' \cdot \mathbf{B}')}\,\mathbf{B}' \otimes \mathbf{B}'. \tag{44}$$

Satisfaction of (14) now requires $< \mathcal{R} >^{-1} = \mathcal{K}$.

The invariant decomposition of stress deviator analogous to (8) is

$$\begin{aligned} \mathbf{S} &= \mathbf{S}^{**} + S_C\mathbf{C}' + S_B\mathbf{B}' \\ &= \mathbf{S}^{**} + \frac{(\mathbf{S} \cdot \mathbf{C}')}{(\mathbf{C}' \cdot \mathbf{C}')}\,\mathbf{C}' + \frac{(\mathbf{S} \cdot \mathbf{B}')}{(\mathbf{B}' \cdot \mathbf{B}')}\,\mathbf{B}', \end{aligned} \tag{45}$$

where the kinematically–determinable $\mathbf{S}^{**}$ lies in a three–dimensional subspace of T_2', and S_C and S_B are the deviatoric stress reactions which must be determined from equilibrium. Finally, the approximations $\mathbf{S} \cdot \mathbf{C}' \doteq \bar{\mathbf{S}} \cdot \mathbf{C}'$ and $\mathbf{S} \cdot \mathbf{B}' \doteq \bar{\mathbf{S}} \cdot \mathbf{B}'$ furnish, through (28), the generalized global equilibrium relation

$$< \mathcal{R} > [\bar{\mathbf{S}}] = < \mathbf{S}^{**} > . \tag{46}$$

4. APPLICATIONS

4.1 Numerical calculations

Because of the incompressibility, the strain rate is vectorized to five independent components referred to a fixed cartesian basis:

$$\mathbf{D} \rightarrow \vec{D} \equiv \left\{(D_{22} - D_{11})/\sqrt{2}, \sqrt{3/2}D_{33}, D_{23}/\sqrt{2}, D_{13}/\sqrt{2}, D_{12}/\sqrt{2}\right\}^T .$$

All other deviatoric tensors are also vectorized in the above convention.

The solution procedure is as follows. Once an estimate of $\bar{\mathbf{D}}$ is known, the local stretching $\mathbf{D}$ is calculated from (22), since both local orientation and global texture are assumed to be known instantaneously. The non-linear relation (11) between $\mathbf{D}$ and the reduced stress $\mathbf{S}^*$ is solved by the Newton-Raphson method to obtain $\mathbf{S}^*$. The global average $< \mathbf{S}^* >$ is then obtained, and (31) is solved to obtain $\bar{\mathbf{S}}$. If global stress boundary conditions are satisfied to sufficient tolerance, the solution is accepted; otherwise, Newton–Raphson corrections to the work–conjugate components of $\bar{\mathbf{D}}$ are made, and the procedure is repeated. Once global conditions are met, the remaining portion of $\mathbf{S}$ is obtained from assumption (30) when it is required. Local updating of lattice orientation proceeds by constructing an orthogonal tensor $\mathbf{Q}^L = exp\{\Delta t\,(\mathbf{W} - \mathbf{W}^p)\}$, where Δt is a small time increment, and the spin tensors are obtained from (23) and (26). Lattice tensors (*e.g.*, $\mathbf{R}^a$, $\mathbf{A}^a$, $\mathbf{C}'$) are then updated according to $\mathbf{C}'(t + \Delta t) = \mathbf{Q}^L\mathbf{C}'(t)\mathbf{Q}^{L^T}$, *etc.* In the updated configuration, the procedure is repeated for the next increment. Typically, global deformation increments of one percent are used. Similar procedures are used for the case of two constraints.

Initial isotropic distributions of lattice orientation are constructed using random numbers. A check on the isotropy of the initial texture was obtained from (41); typically the numerical value of $< P >$ deviated from $\frac{4}{5}I$ by less than two percent.

4.2 Application to Hexagonals

The slip systems reported to be activated in different hexagonal crystals (GROVES and KELLY, 1963) are of two types — slip systems with **a** as Burger's vector: basal slip $\{0001\} < \bar{2}110 >$, prismatic slip $\{01\bar{1}0\} < \bar{2}110 >$, and pyramidal slip $\{01\bar{1}1\} < \bar{2}110 >$; and slip systems with $(\mathbf{a} + \mathbf{c})$ as Burger's vector. TOMÉ and KOCKS (1985) analyzed single crystal plasticity of hexagonals yielded by different types of slip and twinning systems.

Since the Burger's vector **a** of basal and prismatic systems lies in the basal plane, these two sets of systems together comprise only four linearly independent slip systems. For the same reason, the addition of the pyramidal slip $\{01\bar{1}1\} < \bar{2}110 >$ does not supply the missing degree of freedom (*i.e.*, no plastic deformation along the **c**–axis). The additional mechanisms which can supply the missing degree of freedom are pyramidal slip with Burger's vector $< \mathbf{a} + \mathbf{c} >$ or certain twinning systems, TOMÉ and KOCKS (1985).

HUTCHINSON (1977) applied self-consistent and upper bound models to hexagonal polycrystals with isotropic texture and with an ideal lattice ratio $c/a = 2\sqrt{(2/3)}$ to predict the uniaxial reference stress $\bar{\sigma}_0$ in the following uniaxial power law creep equation:

$$\bar{D}^{eq} = \dot{\gamma}_0 \left(\bar{\sigma}^{eq}/\bar{\sigma}_0\right)^n, \tag{47}$$

or, equivalently,

$$\bar{\sigma}_0 = \bar{\sigma}^{eq} \left(\bar{D}^{eq}/\dot{\gamma}_0\right)^{-1/n}, \tag{48}$$

where $\bar{D}^{eq} \equiv \sqrt{\frac{2}{3}\bar{\mathbf{D}} \cdot \bar{\mathbf{D}}}$ and $\bar{\sigma}^{eq} \equiv \sqrt{\frac{3}{2}\bar{\mathbf{S}} \cdot \bar{\mathbf{S}}}$ are the macroscopic equivalent uniaxial tensile strain rate and equivalent tensile stress, respectively, $\dot{\gamma}_0$ is the reference shear rate of the single crystal, and $n = 1/m$, where m is the rate sensitivity exponent. HUTCHINSON considered basal and prismatic, as well as pyramidal slip $\{11\bar{2}2\} < \bar{1}\bar{1}23 >$. He compared self-consistent and upper bound (TAYLOR) results for different rate sensitivities and differing ratios of critical resolved shear stresses on different systems. When the critical resolved shear stress on the pyramidal system is infinite (*i.e.*, pyramidal slip is omitted), the upper bound calculation fails because of the inextensibility constraint in the c direction. However, in this case he was able to obtain results from the self–consistent model.

Here we compare results from the CH model with HUTCHINSON'S in the case of four independent systems only (basal and prismatic systems). Direct comparisons are made for exponents $n = 1$ and $n = 3$ and for the critical resolved shear stress ratio $\tau_p/\tau_b = 10$, where τ_b and τ_p are critical resolved stresses for basal and prismatic systems, respectively. The polycrystalline aggregate consists of 248 randomly oriented single crystals, resulting in an isotropic texture.

Results of the tensile reference stress $\bar{\sigma}_0$, normalized by τ_p, are given in Table 1, as are HUTCHINSON'S results. In the linear ($n = 1$) case, the model prediction falls between the self–consistent and Hashin–Shtrikman lower bound, approximately 78% of

the self-consistent value. For $n = 3$, the self–consistent estimate more than doubles, compared to the $n = 1$ case, while the CH estimate increases modestly by only ten percent above its $n = 1$ value. HUTCHINSON (1977) noted that there are reasons to suspect that the self–consistent model overestimates $\bar{\sigma}_0$ when pyramidal slip is absent, so the current results may be more accurate.

Figure 2 shows the variation of the normalized reference stress versus the slip system hardness ratio τ_b/τ_p for $n = 1$ and $n = 3$ as predicted by the present model. Results for $n > 3$ differ only slightly from those of $n = 3$. We note that the value of $n = 3$ and "hard" prismatic systems (small τ_b/τ_p) corresponds to ice crystals (HUTCHINSON, 1977; WEERTMAN, 1973; ASHBY and DUVAL, 1985).

4.3 Application to Olivine

Olivine is a crystalline mineral which is believed to be the major constituent of the upper mantle. Strong seismic anisotropy has been observed in the upper mantle beneath both oceanic and continental crust. At high pressures, where microcracks are closed, it is possible that seismic anisotropy could be due to preferred crystalline orientation, or texture. Recently TAKESHITA, *et al.*, (1989) have begun to model the development of polycrystalline deformation texture in olivine.

Olivine has an orthorhombic crystal lattice. Several experiments have been carried out to determine operative slip systems at different temperatures (CARTER and AVÉ LALLEMANT, 1970; DURHAM and GOETZ, 1977; RALEIGH, 1968). TAKESHITA, *et al.*, (1989) summarize the slip systems into two classes; class A for low temperature, and class B for higher temperature, and estimate the resistances for these systems. They

note that the class B systems and resistances are based on single crystal experiments, while the class A systems should be viewed as more tentative. These systems are summarized in Table 2. Both classes have only three independent slip systems, allowing no inelastic stretching along (unit) crystallographic directions **a**, **b**, and **c** (*i.e.*., normal strain components referred to crystallographic axes cannot be accommodated by slip).

In order to use the TAYLOR formalism, TAKESHITA, *et al.*, proposed that the normal strains (strains in crystallographic directions) are accommodated by dislocation climb while shear strains (as referred to crystallographic axes) are accommodated by slip.[1] The neglected normal strain components were presumed to make no contribution to textural evolution. They also used the self–consistent model of MOLINARI, *et al.*, (1987) to predict texture of olivine deformed by simple shear and compared results to the TAYLOR model predictions. For neither model was the predicted polycrystalline stress strain response reported.

Here we use the nonhardening CH model to predict the behavior of olivine and compare our results to those of TAKESHITA, *et al.* Since there are only three independent slip systems for either of the two classes of slip systems, we use the two–constraint version of the model outlined in section 3.4. The normal stretching components are zero along the crystallographic axes: $\mathbf{a} \cdot \mathbf{Da} = \mathbf{b} \cdot \mathbf{Db} = \mathbf{c} \cdot \mathbf{Dc} = 0$. Because of assumed incompressibility, the three normal strain constraints are reduced to only two independent deviatoric constraints, which can be expressed as

$$\mathbf{D} \cdot \mathbf{B}' = 0, \tag{49}$$

[1] Procedures locally requiring certain deformation components to equal the corresponding macroscopic average components, while simply ignoring (in a mechanics sense) the other components, have collectively come to be termed "relaxed constraint" models.

$$\mathbf{D} \cdot \mathbf{C}' = 0, \tag{50}$$

where $\mathbf{B}' \equiv (\mathbf{b} \otimes \mathbf{b} - \mathbf{a} \otimes \mathbf{a})$ and $\mathbf{C}'$ is given by (3).

We considered the olivine behavior and development of anisotropy under conditions of both simple shearing and plane strain compression at high temperature (class B). The initial texture, consisting of 248 randomly oriented single crystals, is isotropic and is represented by pole figures in Fig. 3. We chose a value of $n = 5$ as did TAKESHITA, *et al.*, (1989). The predicted stress strain curves are given in Fig. 4 for both plane strain compression and simple shear. The macroscopic equivalent tensile stress, $\bar{\sigma}^{eq}$, is normalized by τ_0, the initial resistance of the easiest slip system. The macroscopic equivalent strain is defined as $\bar{\epsilon}^{eq} \equiv \int \bar{D}^{eq}\, dt$.

The texture developed under simple shear is shown in Fig. 5, where the sense of shear is indicated by the arrows. This texture is in agreement with those obtained by TAKESHITA, *et al.*, and with a texture which has been observed in naturally deformed olivine (MERCIER, 1985). Texture developed during plane strain compression, Fig. 6, as predicted by the present model, is also in agreement with the predictions of TAKESHITA, *et al.* Unfortunately for purposes of comparison, at present there seems to be no available experiments on polycrystalline olivine documenting texture evolution from an initially isotropic texture under simple shear or plane strain compression.

4.4 Application to HDPE

High density polyethylene (HDPE) is a semi-crystalline polymer with crystallinity typically between 70% and 80%. In order to apply the present model in a highly idealized manner to HDPE, we neglect the contribution of the amorphous phase by

assuming an "ideally crystalline" polyethylene (100% crystallinity). We further neglect the important morphological texture of the material, which, in the macroscopically isotropic case, usually consists of spherulitic regions containing crystalline lamellae and amorphous interlamellar domains of highly correlated *local* orientation, but of random orientaion when averaged over the spherulite.

Plastic deformation of single crystal (lamella) HDPE was reviewed by BOWDEN and YOUNG (1974) and by HAUDIN (1982). The crystalline domains (lamellae) form an orthorhombic lattice with the c axis in the polymer chain direction. The crystals can deform by slip, twinning or martensitic transformation. In this application we consider only plasticity by slip. The possible slip systems are chain slip (axis c is Burger's vector) and transverse slip (Burger's vector perpendicular to c axis). Table 3 summarizes all possible slip systems, along with corresponding estimated normalized deformation resistances. Together, these provide only four independent slip systems, allowing no plastic extension in the c direction (chain direction). The possible twinning modes, which are not included in our calculations, do not provide an additional independent system.

We used the CH model with one constraint to predict the behavior and texture evolution of an ideally 100% crystalline HDPE under both tension and simple shear. The initial texture, again consisting of 248 randomly oriented single crystal orientaions, is isotropic, as indicated by the pole figure shown in Fig. 3. The value of n is taken as 17, which corresponds approximately to the strain rate sensitivity exponent $m = 0.06$ obtained experimentally at room temperature by G'SELL and JONAS (1979) in tests of spherulitic HDPE. In view of the small lamellar thicknesses ($\sim 20\,nm$), it was felt that strain hardening by dislocation interaction within the lamellae was likely to be

insignificant, so no hardening of slip system critical resolved shear stress was included.

Equivalent stress strain curves for simple shear and for tension are given in Fig. 7. Stress is normalized by the critical resolved shear stress for chain slip. Evidently, textural hardening of HDPE is very important in tension but not in simple shear. This result is in excellent agreement with the experimental results of G'SELL, *et al.*, (1982).

The texture developed during tension is a fiber texture, Fig. 8, with chain direction (c–axis) parallel to the tension direction. Clearly, this distribution of the inextensible chain directions is responsible for the dramatic upturn in the tensile stress strain curve of Fig. 7.

The texture developed by simple shear is shown in Fig. 9, where it is noted that a reversed sense of shear (as compared to that used for olivine in Fig. 5) has been adopted. In Fig. 9a, at a shear of $\gamma = 2.16$, a sharp c–axis texture component forms along the material fiber of maximum stretch, and the two other crystallographic axes are almost randomly oriented around c (fiber texture). Figure 9b, at a shear of $\gamma = 2.6$, shows further sharpening of the c–axis texture in a direction closer to the shearing direction. The fact that the c–axis rotates toward the direction of maximum stretch, which itself is tending toward the shearing direction with ongoing shear, allows most of the deformation to be accomodated by chain slip (easy slip). This explains why the textural hardening is very weak in simple shear. On the contrary, when the HDPE becomes textured under tension, it exhausts available deformation mechanisms and the requisite driving stress tends to infinity.

Results from more sophisticated composite inclusion models (AHZI, PARKS and

ARGON, 1989; PARKS and AHZI, 1989), in which we accounted for effects of the interlamellar amorphous phase in HDPE, showed qualitatively similar stress strain behavior and texture evolution. In the latter models, however, equivalent sharpness textures were obtained at consistently higher strains than in the current calculations. This indicates that a primary role of the amorphous material in HDPE is to provide additional straining without substantial effect on crystallographic texture.

5. DISCUSSION

We have clearly identified the special constitutive features of rigid–viscoplastic single crystals which do not possess five independent slip systems. In addition to the relatively well–known kinematic constraint, there is a corresponding indeterminacy in the deviatoric stress. Based on these observations, we have constructed a simple TAYLOR–type polycrystalline model which accounts for the local kinematic constraints, as well as providing a means for dealing with the "kinematically indeterminant" part of the local stress deviator. As examples of the broad applicability of the model, we applied it to various problems of polycrystalline deformation and texturing in kinematically deficient crystals of hexagonal and orthorhombic symmetry. These examples were intended simply to demonstrate the new model, rather than as comprehensive, or even complete, studies of particular problem areas. Further applications of the model are underway, and will be reported.

A primary reason for the success of the model is that, like the self–consistent formulations, it imposes far less stringent kinematic conditions on individual inclusions than uniform deformation. As in the self–consistent models, global compatibility (in the form of macroscopic deformation equalling the volume average of local deformation) is preserved, but local compatibility is not addressed. While such "disregard" for local compatibility may seem to be a limitation of these approximate models, a rigorous study would require higher order statistical information regarding the microstructure, as well as recognizing the inhomogeneity of plastic deformation within grains (ASARO, 1983a,b).

In preserving the volume–average character of deformation, a macroscopic projec-

tion tensor, $< P >$, played a prominent role. We presumed that this diagonally symmetric fourth order tensor was invertible; *i.e.*, that it mapped T_2' to itself. In certain extreme (Dirac–like) textures, such as the fiber textures displayed in Figs. 8 and 9, $< P >$ itself becomes degenerate, spanning only $T_{2\perp C}'$. The simple shear calculations could be continued without substantial difficulty, but tensile deformation was extinguished. In any event, the numerical condition of $< P >$ can become an issue at sharp texture.

The tensor $< P >$ also played an important role in enforcing the volume average condition on the stress deviator. This occurred because the local constraint stress was approximated by the corresponding component of the macroscopic stress. We are not aware of rigorous justifications for making this assumption. Rather, we sought simply to provide for some measure of equilibrium between the constrained inclusion and its macroscopic surroundings. Perhaps a related (though less sophisticated) assumption might attempt to account for pressure sensitivity of rigid–viscoplastic polycrystalline slip by assuming local pressure within an inclusion to equal the global average pressure, which in turn could be deduced from traction boundary conditions.

We generalized the formulation to account for two (or more) deviatoric constraints within grains (three or fewer independent systems), and applied it to deformation texturing in the mineral olivine. Formally, the methodology could be extended to a single slip system within each grain, but we reserve judgment on its utility in that limit. For example, in the hexagonal reference stress study, we found indications of a non–zero limit for $\bar{\sigma}_0/\tau_p$ as τ_b/τ_p approached zero, Fig. 2. On the other hand, one could argue that in this limit, prismatic slip would be "infinitely" more difficult than basal slip, so that only the two independent basal systems should be retained (three

constraints). In that event, $\bar{\sigma}_0$ would scale with the retained τ_b.

ACKNOWLEDGMENTS

This work was supported by a DARPA U.R.I. program under ONR Contract # N00014-86-K-0768. We are pleased to acknowledge discussions with A. S. Argon, R. E. Cohen, and H. Song. Computations were performed in part on a Data General MV–10000 computer donated to MIT by the Data General Corporation.

REFERENCES

AHZI, S., PARKS, D. M. and ARGON, A. S.	1989	*Proc. ACS Symposium on Computer Simulation of Polymers*, Orlando
ASARO, R.J.	1983a	*J. Appl. Mech.* **50**, 921.
ASARO, R. J.	1983b	*Advances in Applied Mechanics* **23**, 1., Academic Press, New York.
ASARO, R. J. and NEEDLEMAN, A.	1985	*Acta Met.* **33**, 923.
ASARO, R. J. and RICE, J. R.	1977	*J. Mech. Phys. Solids* **25**, 309.
ASHBY, M. F. and DUVAL, P.	1985	*Cold Reg. Sci. Techn.* **11**, 285.
BOWDEN, P. B. and YOUNG, R. J.	1974	*J. Mat. Sci.* **9**, 2034.
CARTER, N. L. and AVÉ LALLEMANT, H. G.	1970	*Geol. Soc. Am. Bull.* **81**, 2181.
DURHAM, W. B. and GOETZE, C.	1977	*J. Geol. Res.* **82**, 5131.
GROVES, G. W. and KELLEY, A.	1963	*Phil. Mag.*, **8**, p. 877.
G'SELL, C., BONI, S. and SHRIVASTAVA, S.	1983	*J. Mat. Sci.*, **18**, p. 903.
G'SELL, C. and JONAS, J. J.	1979	*J. Mat. Sci.*, **14**, p. 583.
HAUDIN, J. M.	1982	*Plastic Deformation of Amorphous and Semi-Crystalline Materials*, p. 291, Eds. B. ESCAIG and C. G'SELL Les Editions de Physique, Les Ulis.
HILL, R.	1956	*J. Mech. Phys. Solids* **5**, 66.
HILL, R.	1965	*J. Mech. Phys. Solids* **13**, 89.
HILL, R.	1972	*Proc. R. Soc. Lond.* **A326**, 131.
HUTCHINSON, J. W.	1970	*Proc. R. Soc. Lond.* **A319**, 247.
HUTCHINSON, J. W.	1976	*Proc. R. Soc. Lond.* **A348**, 101.
HUTCHINSON, J. W.	1977	*Met. Trans.* **8A**, 1465.
MERCIER, J.-C. C.	1985	*Preferred Orientation in Deformed Metals and Rocks: An Introduction to Modern Texture Analysis*, p. 407, Ed. H.-R. WENK, Academic Press, New Y
MOLINARI, A., CANOVA, G. R., and AHZI, S.	1987	*Acta Met.* **35**, 2983.
ONAT, E. T. and LECKIE, F. A.	1988	*J. Appl. Mech.* **55**, 1.
PAN, J. and RICE, J. R.	1983	*Int. J. Solids Struct.* **19**, 973.
PARKS, D. M.	1989	ms. in preparation.
PARKS, D. M. and AHZI, S.	1989	ms. in preparation.
RALEIGH, C. B.	1968	*J. Geol. Res.* **73**, 5391.
TAKESHITA, T. C., WENK, H.-R., CANOVA, G. R., and MOLINARI, A.	1989	*Deformation Mechanisms in Minerals and Ceramics*, Eds. D. J. BARBER and MEREDITH, Allen and Unwin, London.
TAYLOR, G.I.	1938	*J. Inst. Metals* **62**, 307.
TOMÉ, C., and KOCKS, U. F.	1985	*Acta Met.* **33**, 603.
WEERTMAN, J.	1973	*Physics and Chemistry of Ice*, p. 320, Eds. E. WHALLEY, S. J. JONES, and L. W. GOLD, Royal Society of Canada, Ottowa.

$(\tau_b/\tau_p = 1/10)$	$\bar{\sigma}_0/\tau_p$ $(n = 1)$	$\bar{\sigma}_0/\tau_p$ $(n = 3)$
Taylor Model	∞	∞
H.-S. Upper Bound	∞	∞
Self-Consistent	1.75	3.9
H.-S. Lower Bound	0.74	
Sachs Model	0.45	
CH Model	1.37	1.49

Table 1: Macroscopic tensile stress reference values, normalized by τ_p, in an isotropic polycrystal of hexagonal single crystals without pyramidal slip. Comparison of CH predictions to results of HUTCHINSON (1977) for the case $\tau_b/\tau_p = 1/10$.

	slip system	normalized resistance
class A	{110}[001]	1.
	{011}[100]	1.
class B	(010)[100]	1.
	(001)[100]	1.3
	(010)[001]	2.7

Table 2: Slip systems of olivine and their corresponding normalized initial critical resolved shear stresses.
A: Low temperature; B: High temperature
(after TAKESHITA, *et al.*, 1989).

	slip system	normalized resistance
Chain slip	(100)[001]	1.
	(010)[001]	1.
	{110}[001]	1.
Transverse slip	(100)[010]	1.1
	(010)[100]	1.4
	$\{110\} < 1\bar{1}0 >$	1.8

Table 3: Slip systems of polyethylene and estimates of their corresponding normalized initial critical resolved shear stresses.

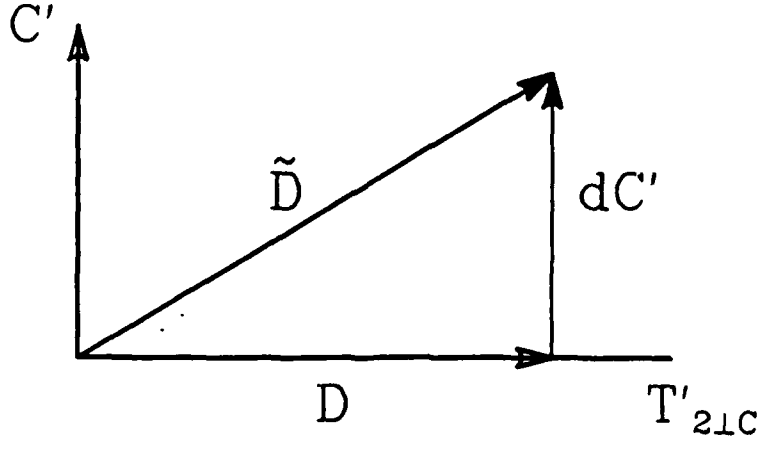

Figure 1: Schematic representation of local strain rate in reduced space.

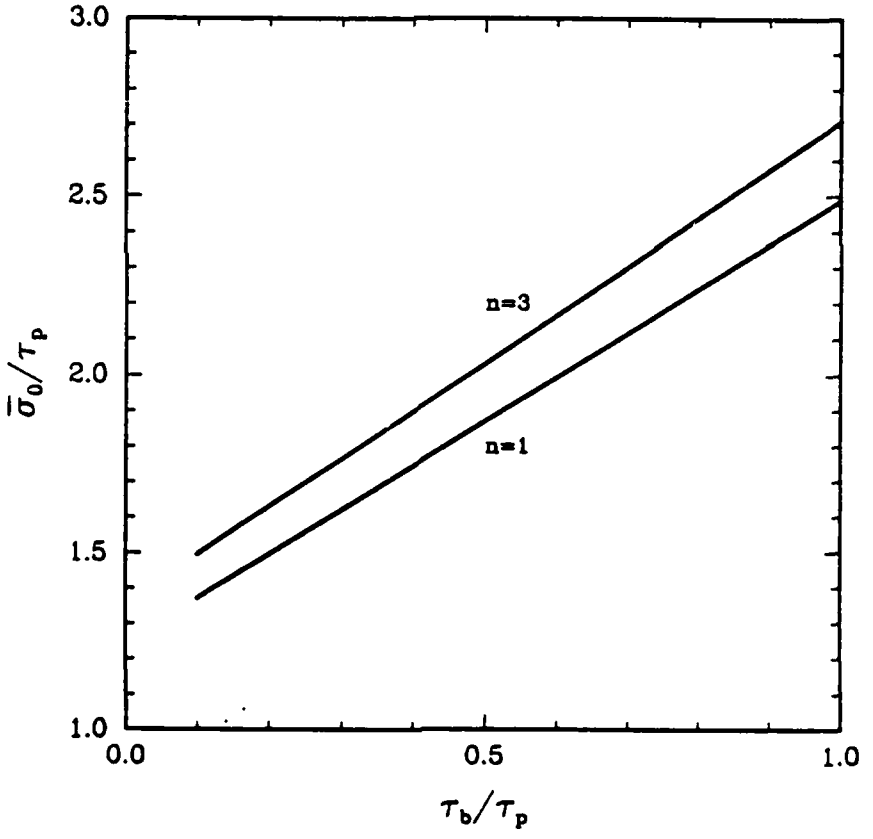

Figure 2: Macroscopic reference stress for isotropic HCP polycrystals having only basal and prismatic slip.

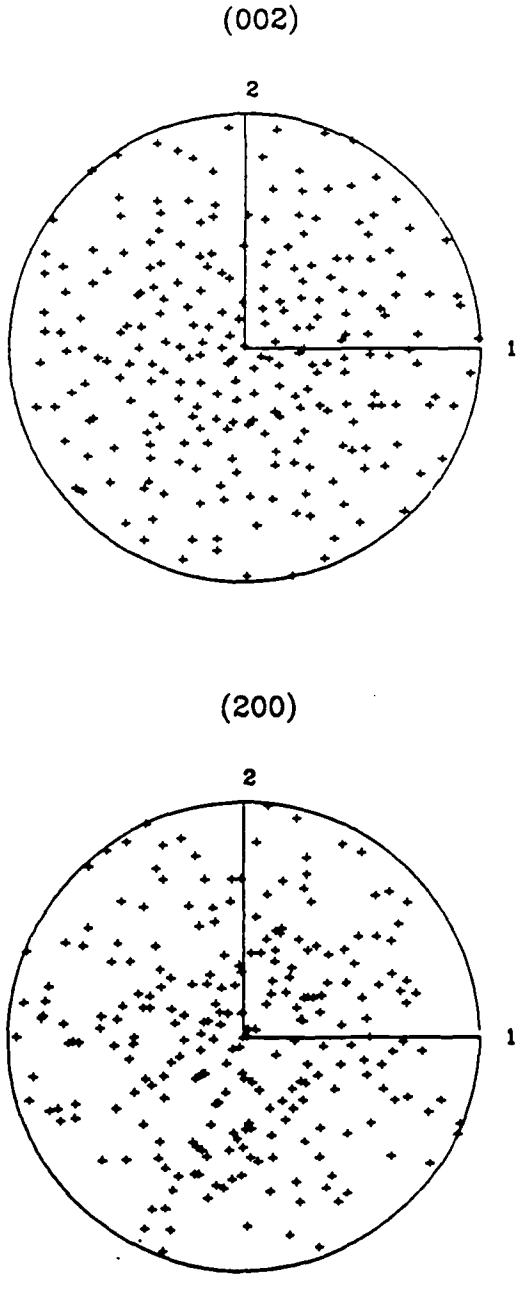

Figure 3: (002) and (200) pole figures representing the initial isotropic texture (248 orientations).

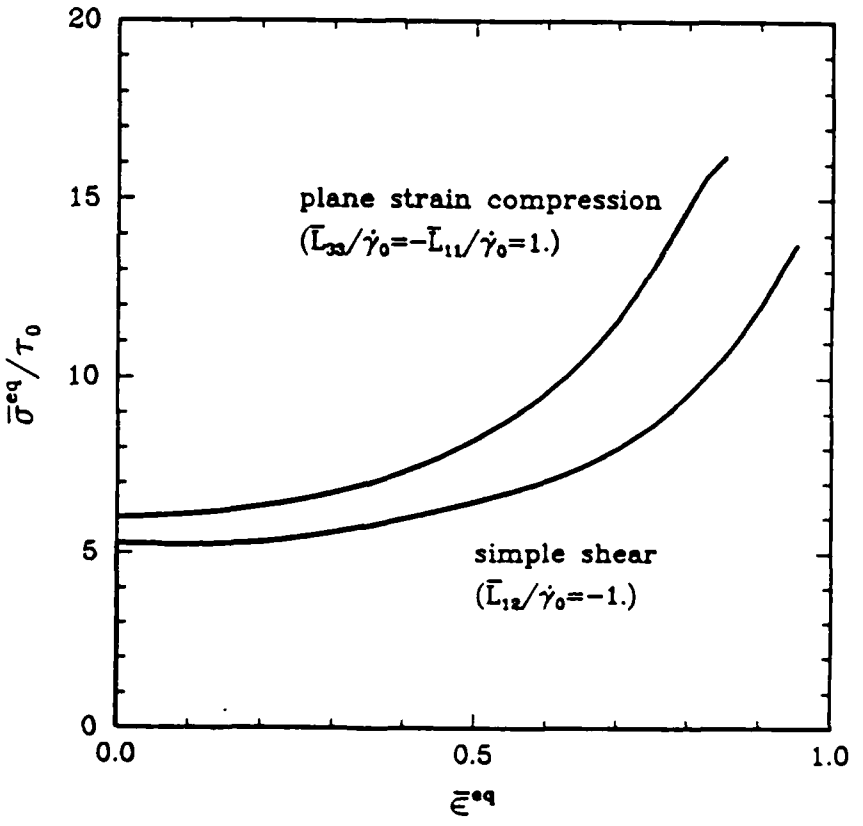

Figure 4: Macroscopic equivalent stress–strain curves for olivine.

(001)

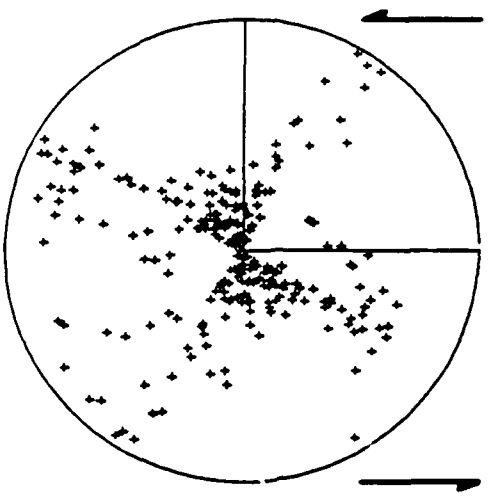

(010)

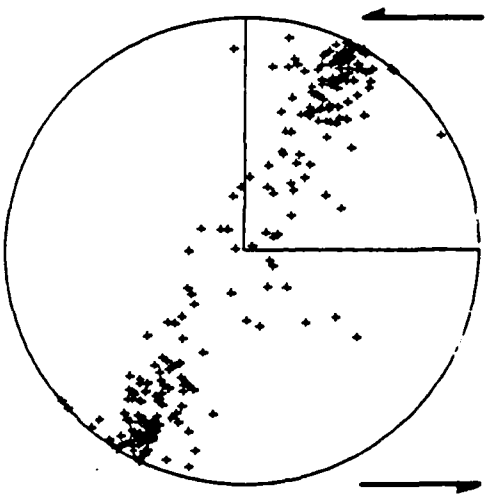

Figure 5: Predicted (001) and (010) pole figures for simple shear of olivine (γ=1.3).

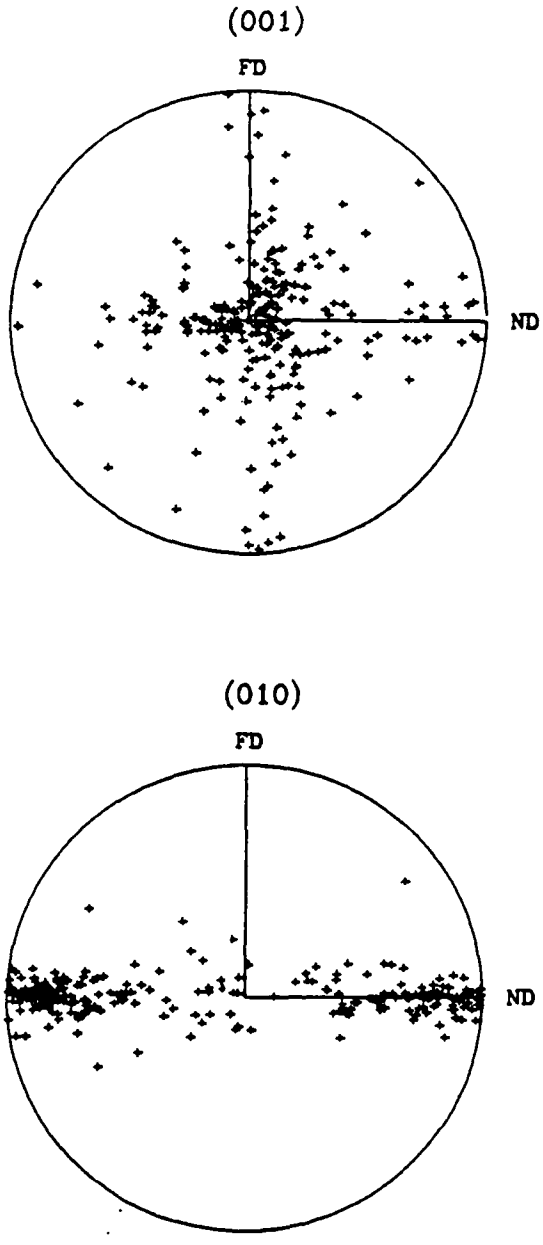

Figure 6: (001) and (010) pole figures for plane strain compression of olivine ($\bar{\epsilon}^{eq}$=.75).
(ND= normal direction; FD= free direction).

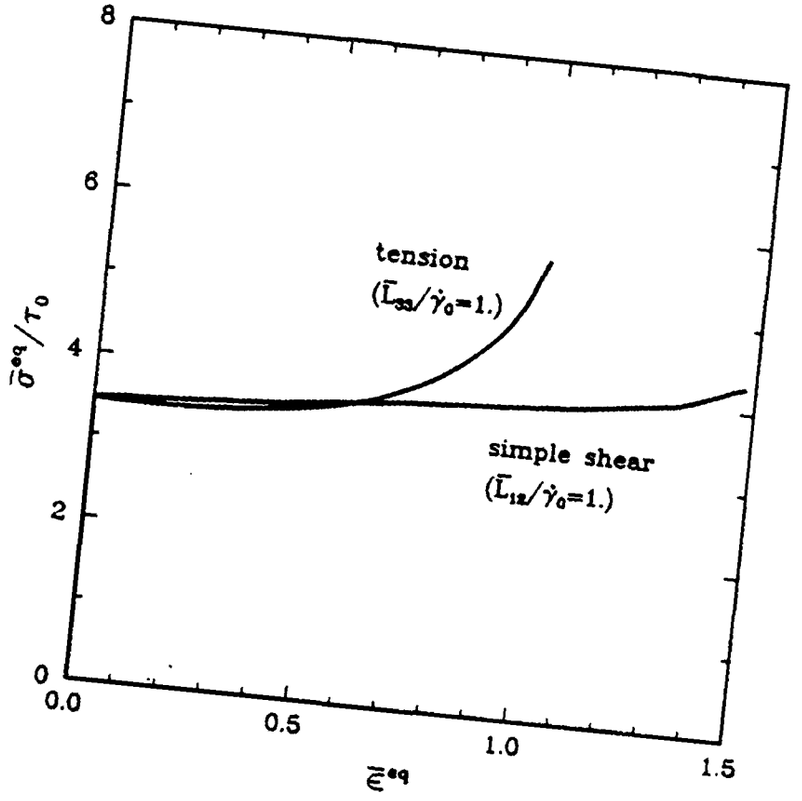

Figure 7: Macroscopic equivalent stress–strain curves for idealized 100% crystalline HDPE.

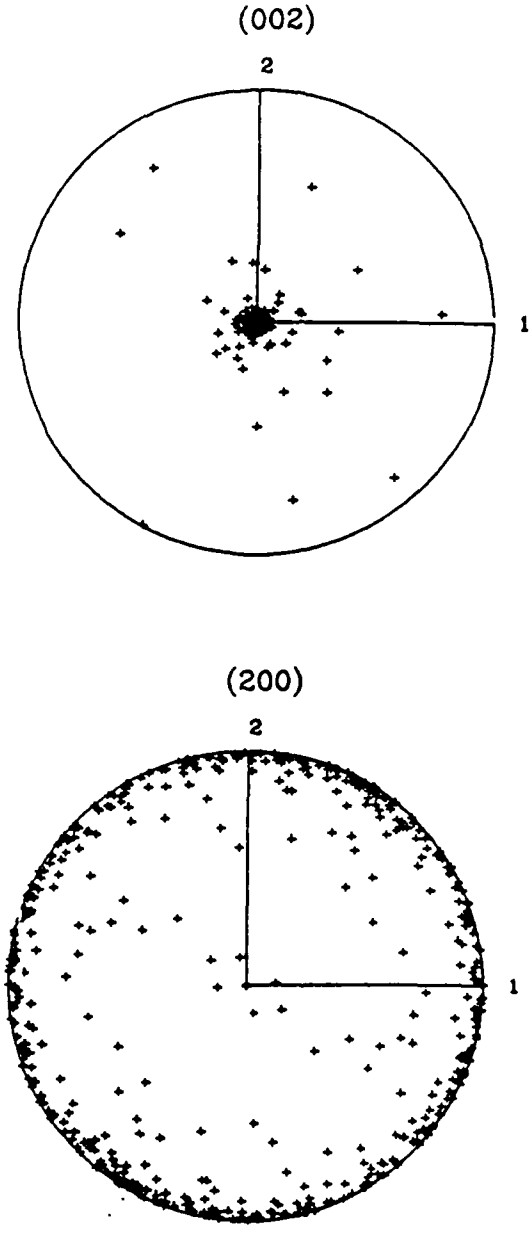

Figure 8: Predicted (002) and (200) pole figures (fiber texture) for tension of 100% crystalline HDPE. $\bar{\epsilon}^{eq}=1$. (axis 3 = tension direction).

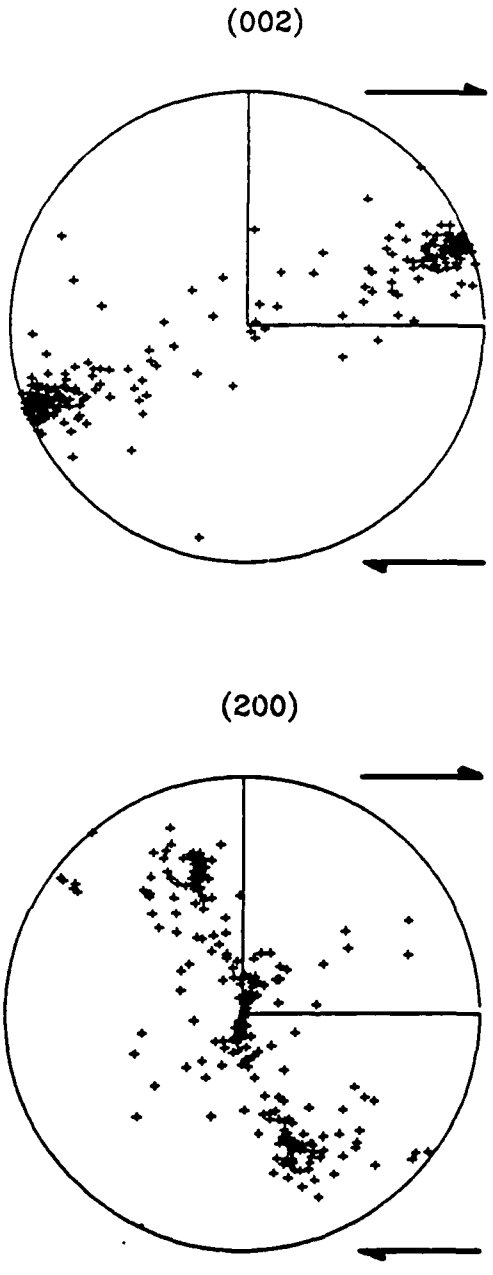

Figure 9–a: Predicted (002) and (200) pole figures for simple shear of 100% crystalline HDPE. (γ=2.16).

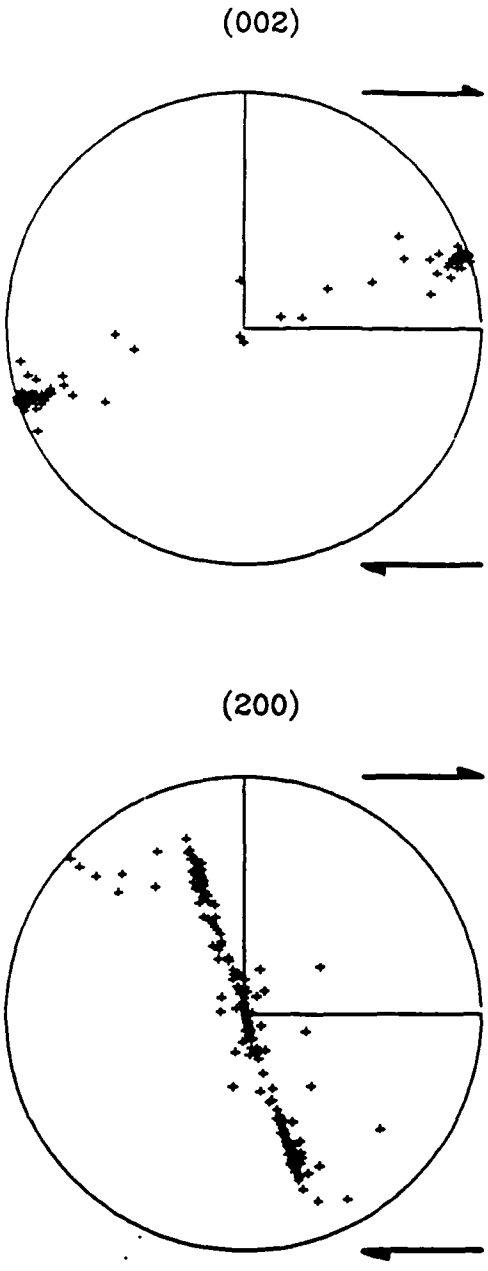

Figure 9–b: Predicted (002) and (200) pole figures for simple shear of 100% crystalline HDPE. (γ=2.6).